Fowler–Nordheim tunnelling in TiO$_2$ films grown by atomic layer deposition on gold substrates

Indrek Jõgi[a], Jaan Aarik[b], Viktor Bichevin[b], Henn Käämbre[b], Matti Laan[a], and Väino Sammelselg[b]

[a] Institute of Experimental Physics and Technology, University of Tartu, Tähe 4, 51010 Tartu, Estonia; laan@ut.ee
[b] Institute of Physics, University of Tartu, Riia 142, 51014 Tartu, Estonia; henn@fi.tartu.ee

Abstract. Current–voltage characteristics were measured for Au–TiO$_2$–Ag structures with TiO$_2$ layers of 30–180 nm thickness. In the case of negative bias on the Au electrode, the conduction currents through TiO$_2$ layers follow over several orders of magnitude the Fowler–Nordheim formula for the field emission, allowing attribution of the bulk currents to tunnelling, seemingly through a Schottky barrier at the Au–TiO$_2$ junction. In the case of reversed polarity the currents are also observed, but cannot be interpreted as tunnelling.

Key words: titanium dioxide, thin films, electrical properties, Fowler–Nordheim plots, tunnelling currents.

1. INTRODUCTION

Titanium dioxide has found wide application as a valuable pigment in paints, plastic goods, paper, etc. [1]. Its world production amounts to 4 million tonnes. In particular, it is extensively used in the pharmaceutical industry, specifically as a catalyst for photoinduced reactions, protecting our skin from harmful influences of sun radiation. Attempts have been made to use it in the conductometric gas (e.g. oxygen) sensors [2] and as a high-*k* gate insulator [3]. Very recently it was included into a novel merbromin/Au/TiO$_2$/Ti photovoltaic device (solar cell) [4]. In [5] it is shown that a TiO$_2$ film, covering a point electrode in a negative corona gap, facilitates the occurrence of the discharge. Last but not least – an efficient planar cold cathode, based on TiO$_2$ ultrathin film coatings on metal substrates, has been recently developed by Vu Thien Binh and associates [6–8]. These cold

cathodes are far more technological, run prettily in a lower vacuum and at lower voltages than the conventional ones. Technologically promising results of the above authors stimulated also our present attempt to elucidate further the electrical properties of TiO_2 films.

We report some peculiarities of the current–voltage (I–V) dependence of metal–oxide–metal (MOM) structures containing TiO_2 films. Plotting the I–V characteristics in the Fowler–Nordheim coordinates is the simplest way to reveal the tunnelling currents having a decisive role in the cold cathode performance.

2. EXPERIMENTAL

2.1. Preparation of samples

The MOM structures were prepared on Si(1 0 0) substrates ($5 \times 7 \times 0.3$ mm^3) and they consisted of an Au electrode, a TiO_2 layer, and an Ag counter electrode. Before the formation of the structure the substrates were etched in HF and rinsed in de-ionized water. Then the Au-electrode was deposited by vacuum evaporation. A common thickness of this electrode was around 300 nm.

Titanium dioxide films were grown using atomic layer deposition (ALD), a cyclic process including a periodically repeated series of self-limited surface reactions (in more detail see, e.g., [9,10] and references therein). The deposition was performed in a low-pressure flow-type reactor using $TiCl_4$ as the titanium precursor and H_2O vapour as the oxygen precursor. To synthesize a film, the substrates were alternately exposed to the titanium and oxygen precursors, which were carried to the substrates in a flow of nitrogen gas. Between each exposure the reactor was purged with pure N_2. Thus the process consisted of cycles of exposures to metal and oxygen precursors and the following purge periods. The thickness increment per cycle ranged from 0.053 to 0.078 nm in the case of substrate temperatures (225–275 °C) and precursors used in this work. We applied 500 and 2300 cycles to grow 30 and 180 nm thick films.

2.2. The structure of the samples

To have some conception of the structure and surface morphology of the TiO_2 films, we studied reference samples grown on bare Si(1 0 0) substrates in the same processes as the films for conductance measurements. Reflection high-energy electron diffraction and X-ray diffraction studies revealed anatase phase in all these films.

The surface microstructure of TiO_2 films was studied with a multimode scanning probe microscope AutoProbe CP, PSI/ThermoMicroscopes/Veeco. The microscope worked in the intermittent contact atomic force mode; the samples were exposed in air. Silicon cantilevers (Ultralevers™, PSI), having conical probes and tip radii <10 nm, were used in these studies. The row images of the microscope were filtered for low frequency noise using the image-processing

package IP2 from PSI. The same package was used for calculating root mean square (RMS) roughness of the film surface.
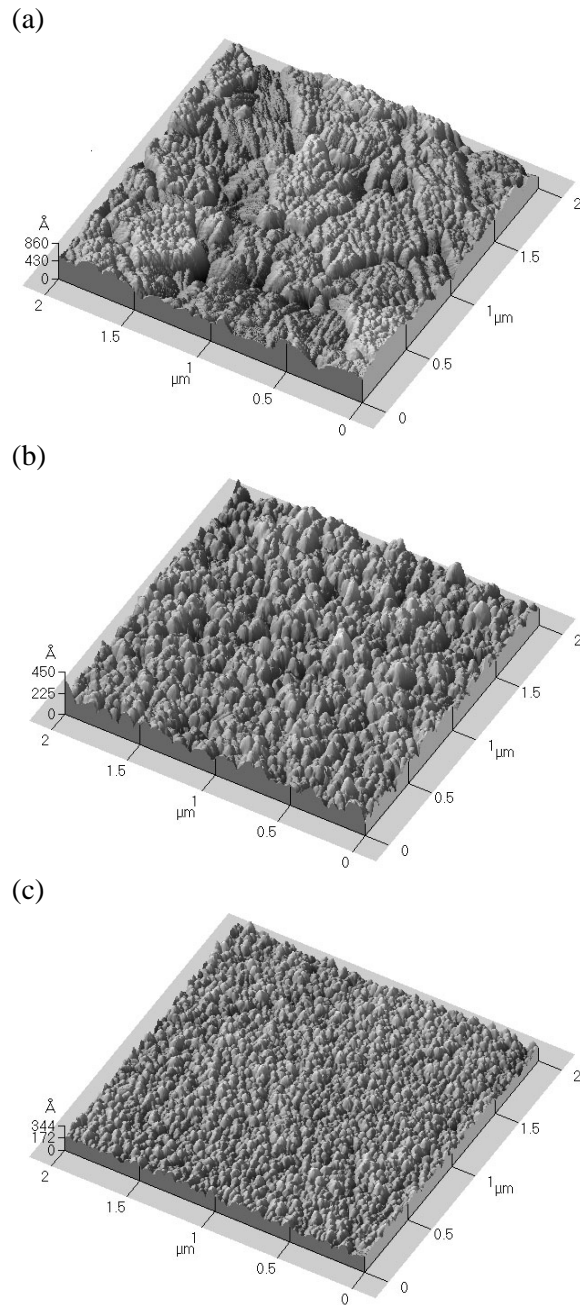
(a)

(b)

(c)

Fig. 1. Surface topography of TiO$_2$ thin films with thicknesses of (a) 180 nm, (b) 80 nm, and (c) 30 nm, depicted with an atomic force microscope in the intermittent contact mode. The RMS roughness of the film surfaces is 11.4, 5.3, and 3.5 nm, respectively.

The obtained images are shown in Fig. 1. As can be seen, the surface roughens drastically with the increasing film thickness. The calculated RMS roughness (R) confirms this trend: it increases from 3.5 nm to 11.4 nm with the increase in the mean film thickness from 30 to 180 nm. Whereas the R of the Si surface was below 1 nm, the RMS thickness variations of the films reached 10% of their total thickness. This result shows that during electrical measurements the local electric fields in the films can differ considerably from those calculated from the applied voltage and mean film thickness. The atomic force microscopy data also show that change of the titanium precursor, i.e. using $Ti(OC_2H_5)_4$ instead of $TiCl_4$, has no noticeable influence on the relative surface roughness of the TiO_2 films grown (Fig. 1b). Our R values agree with these obtained earlier for TiO_2 [9,10], ZrO_2 [11], and HfO_2 [12] films of comparable thickness, grown by ALD. As discussed earlier [9,10], the main reason for the significant surface roughness of TiO_2 films is the evolution of microcrystals during the film growth.

It should be noted that the surfaces of Au-electrodes were much rougher ($R \sim 1$ nm) than the surfaces of silicon substrates ($R \sim 0.2$ nm). Therefore the surfaces of reference films differ significantly from those of the films used for conductivity measurements. Unfortunately, significant contribution of the electrode surface to the total film thickness does not allow reliable observation of additional surface roughening during TiO_2 growth. The results obtained for reference samples indicate, however, that this kind of roughening takes place and, thus, the properties of the $Ag–TiO_2$ interface could depend on the thickness of the TiO_2 film.

2.3. Conductance measurements

The $I–V$ curves were recorded in a standard circuit in the dc mode (Fig. 2, inset). A counter spot electrode needed for these measurements was made by painting a silver suspension onto the TiO_2 layer. The area of the silver spots was ca. 10 mm^2 on the 30 nm thick TiO_2 layers and 2 mm^2 on the 180 nm layers. The sample was connected into the circuit using thin platinum wires that were in contact with the Ag spots on the Au film and the oxide layer.

The current was measured with a multi-range galvanometer M 193 having maximal sensitivity of 4×10^{-8} A per division, and voltage – by a digital voltmeter Щ 4300. The applied voltage was varied in the interval from 10^{-3} to 10 V. The current densities ranged from 10^{-6} to 10 A/cm^2. The measurements were carried out at room temperature in the laboratory atmosphere.

Each measurement series included a stepwise increase in the applied voltage and fixation of the mean current at each step.
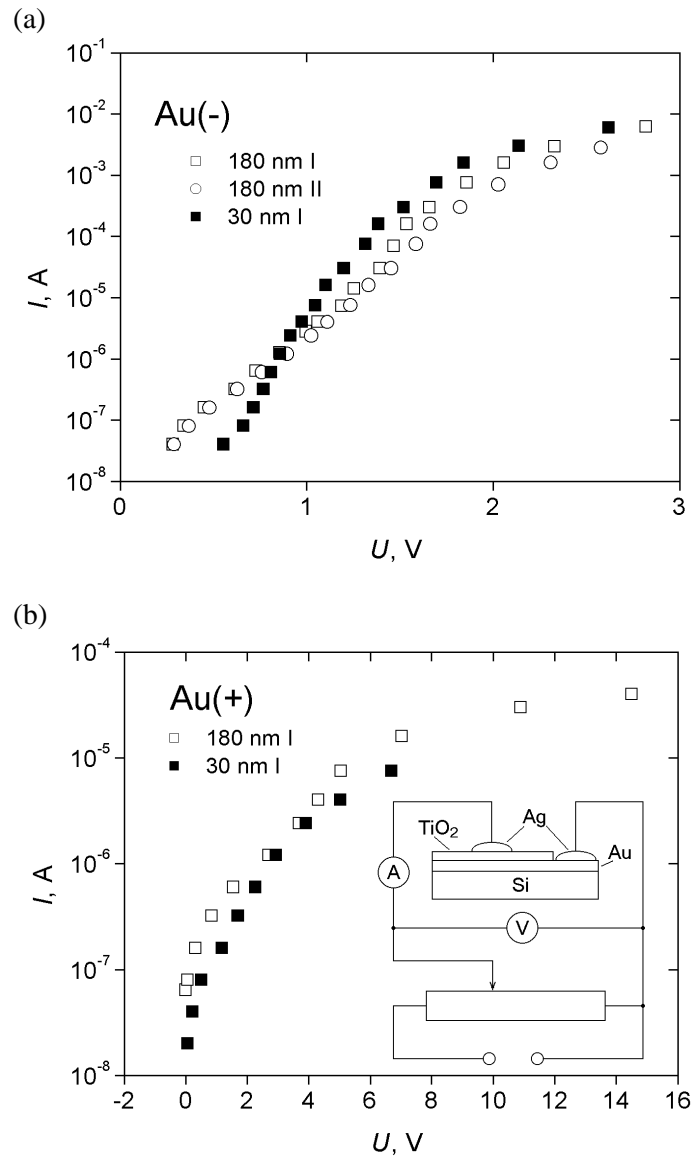
(a)

(b)

Fig. 2. *I–V* characteristics of Au–TiO$_2$–Ag structures including TiO$_2$ layers of different thickness (indicated; I, II – different samples), for (a) Au biased negatively, Au(–), or (b) positively, Au(+). Inset: the measuring circuit diagram.

3. RESULTS AND DISCUSSION

3.1. The current–voltage characteristics

The preliminary conductivity measurements revealed the existence of two types of samples in the patch of specimens at our disposal:

(a) The ones having ohmic, linear *I–V* characteristics. Visual (with a slight magnification) inspection of such films showed that the layers were pierced by discernible pin-holes. During the sedimentation of the Ag suspension the liquid penetrated the film through these voids and formed Au–Ag ohmic contact. These films were excluded from further consideration as erratic and offering no interest.

(b) Higher-quality oxide films without visible holes. These films manifested distinct nonlinearity of the *I–V* characteristics (Fig. 2). As the same figure shows, the *I–V* plots turned out to be different for the differing polarity of the connection of the Au–TiO$_2$–Ag sandwich into the test circuit, i.e., for the cases of negative or positive bias on the Au electrode, further labelled as Au(–) and Au(+) polarity.

3.2. The Au(–) case: a Fowler–Nordheim tunnelling

There is a great variety of the thin film conductance mechanisms (see, e.g., [13]). Attempting to approximate the *I–V* curves by some analytic expression, we revealed that for the Au(–) polarity, the *I–V* dependence can be satisfactorily fitted by the well-known Fowler–Nordheim equation, describing, in general, the field emission current from a metal into vacuum [13,14]:

$$ J = a\phi^{-1}E^2 \cdot \exp\left(-\frac{b\phi^{3/2}}{E}\right) = AE^2 \cdot \exp\left(-\frac{B}{E}\right), \qquad (1) $$

where $A = a\phi^{-1}$ and $B = b\phi^{3/2}$,

$$ a \equiv e^3/8\pi h = 1.541 \times 10^{-6} \text{ A} \cdot \text{eV} \cdot \text{V}^{-2}, $$

$$ b \equiv \frac{4}{3}(2m)^{1/2}/e\hbar = 6.831 \times 10^9 \text{ eV}^{-3/2} \cdot \text{V} \cdot \text{m}^{-1}. $$

Here, J is the current density (A/cm^2), ϕ is the emitter's work function (eV), E is the applied field strength (V/m), e is the elementary positive charge (C), m is the electron effective mass (kg), h is Planck's constant (J · s), and $\hbar = h/2\pi$.

Equation (1) is the Fowler–Nordheim equation in its elementary form, assuming a simple triangular potential barrier for the tunnelling of the field emitted electrons and neglecting some second-order effects. From (1) obviously

$$ \ln\left(\frac{J}{E^2}\right) = \ln A - \frac{B}{E}. \qquad (2) $$

In other words, the Fowler–Nordheim plots (F–N plots)

$$ \ln(J/E^2) = f(1/E) $$

of the *I–V* dependence must be straight lines.

Formula (1) was originally derived to describe the field emission current from sharp metal points or thin wires into vacuum [14]. However, in our case it applies for the conduction current in a MOM sandwich structure. Examining literature, one finds that quite similar cases were revealed as early as in 1967–69 for a Mg–SiO$_2$–Si structure [15,16] and an Al–AlN–Al structure [17]. Very recently the Fowler–Nordheim tunnelling was observed also in magnetron sputtered TiO$_2$ layers [3].

The Fowler–Nordheim equation assumes electron transport from metal to vacuum by tunnelling. Thus, the conductivity in a MOM structure, obeying the same law, should be also of tunnelling nature. As Snow [15] noticed already in 1967, 10 to 10^2 nm oxide layers are much too thick for direct tunnelling through the oxide. Thus, in full accordance with [15,16,18] we believe that the tunnel effect occurs through the field-thinned Schottky barrier at the Au–TiO$_2$ interface and manifests itself in the straight-line F–N plots. (In [3] for Si–TiO$_2$ systems a tunnelling via a SiO$_2$ interlayer is assumed. So as our TiO$_2$ layers are separated from the Si substrate by the gold electrode, this alternative is hardly applicable in our case.)

A highly simplified[1] band diagram in Fig. 3 illustrates the conduction process. Electrons, tunnel-injected into the oxide conduction band, move through the oxide and are picked up by the Ag counter-electrode (cf. [19], p. 454, fig. 10.17). The process can be characterized also as an internal field emission [20].

In our preliminary Fowler–Nordheim tests we estimated the field strength E as $E = U/d$, where U is the voltage applied to the MOM structure and d is the oxide thickness. However, a more refined consideration ([12], p. 635) shows that if a Schottky barrier (blocking contact) is involved, the voltage drop occurs almost entirely on the barrier and the field strength in formulas (1) and (2) should properly be calculated according to the formula
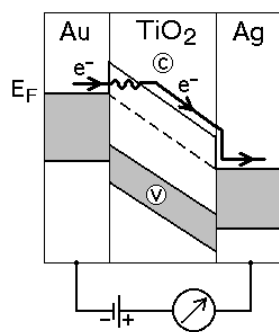

Fig. 3. Simplified band diagram of the electron (e^-) current in an Au–TiO$_2$–Ag structure; E_F is the Fermi level, C the conductance and V the valence band of TiO$_2$.

---

[1] The diagram corresponds to the case E = const. throughout the TiO$_2$ layer, whereas actually the steepest potential gradient should occur inside the barrier region.

232

$$E = \sqrt{\frac{2N_d eU}{\varepsilon\varepsilon_0}} = 0.1902\sqrt{\frac{N_d U}{\varepsilon}} \,. \tag{3}$$

Here, N_d is the concentration of donors (cm^{-3}), ε is the dielectric constant of the oxide, and ε_0 is the electric constant. It should be more correct to write $eU + \phi_0$ instead of eU in formula (3), where ϕ_0 is the initial height of the Schottky barrier. But provided $eU \gg \phi_0$, ϕ_0 can be neglected. This is the case for the voltages used in our work. Besides, the Fowler–Nordheim formula is valid only for a triangular barrier, which the barrier shape approaches better at higher voltages. (Actually, formula (3) gives the E value at the Au–TiO$_2$ interface. Inside the Schottky barrier $E = f(x)$, x being the distance from the interface to an arbitrary point X in the oxide layer.)

Thus, (2) should be rewritten in the form

$$\ln\left(\frac{J}{U}\right) = \ln A - \frac{B}{\sqrt{U}}\,. \tag{4}$$

Figure 4a, b demonstrates the plots of our conductance data in the coordinates of formula (4). Figure 4a shows for the Au(–) polarity a good fit of the experimental points onto the Fowler–Nordheim plot over many decades.

In accordance with the theory is a close coincidence of the F–N plots for the samples of different thickness. Indeed, the field strength at the blocking contact should not depend on the thickness of the dielectric layer [13].

A deviation from the linear F–N plot occurs at lower E (higher $V^{-\frac{1}{2}}$) values (Fig. 4). Especially pronounced is the nonlinearity for the 180 nm films. Analogous nonlinearity is recorded in field-induced external emission from amorphous diamond films [20]. The authors of [20] have shown that this nonlinearity originates from a transition from field emission to thermionic emission as the applied field decreases. Their numerical calculations on the basis of a unified electron emission theory [21], embracing both field and thermionic emission, are consistent with the experimental data. Plausibly, analogous considerations are valid in our case: at lower fields electrons could thermally overcome the Schottky barrier.

We attempted to assess the effective work function ϕ value from the slope of the F–N plots according to formulas (3) and (4). To use formula (3), we need the values of ε and N_d. The authors of [3] and [6] give for TiO$_2$ the values $\varepsilon = 80$ and $\varepsilon = 35$, respectively. Assuming the estimates $\varepsilon = 50$ and $N_d = 10^{18}$ cm^{-3}, one gets $\phi = 0.17$ eV. A similar low ϕ value was estimated in the paper [8] for Pt–TiO$_2$ junctions (see also [20]). There the small ϕ was explained by space charge effects in thin semiconductor films.
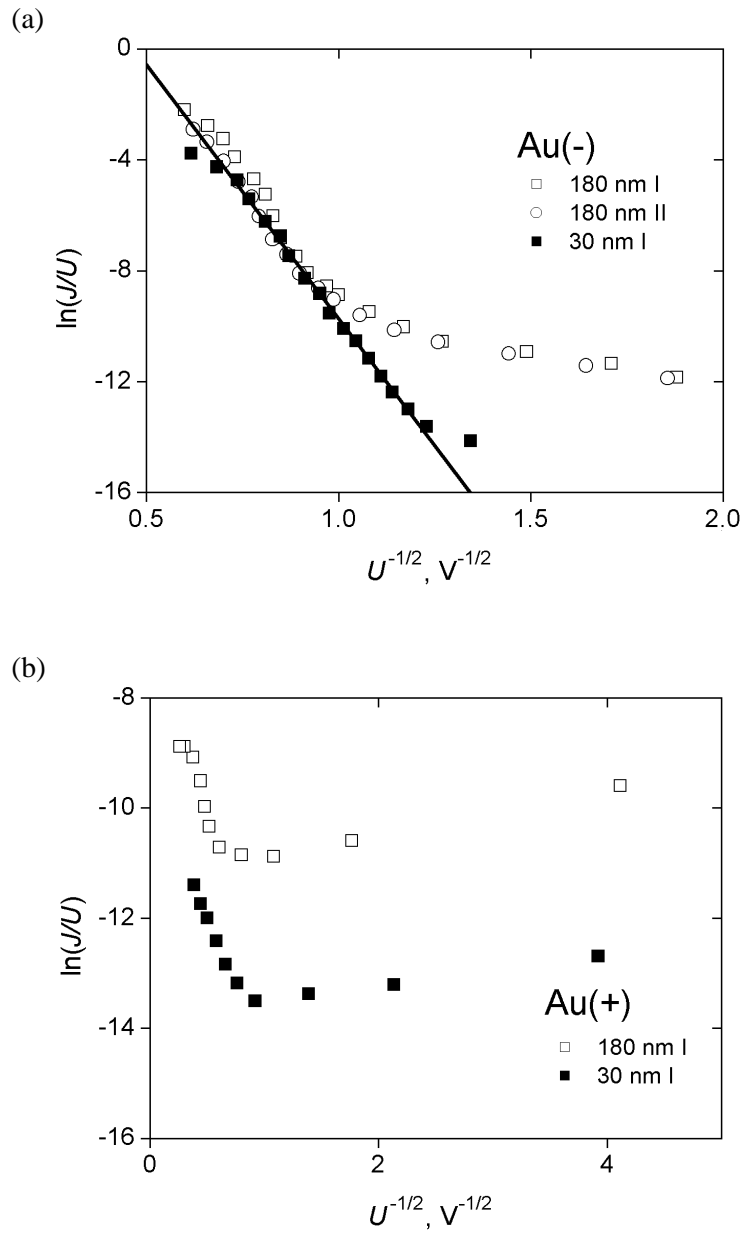
(a)

(b)

Fig. 4. Fowler–Nordheim plots $\ln(J/E^2) = f(1/E)$, $E \sim U^{1/2}$ (see formula (3)), for currents through Au–TiO$_2$–Ag structures including TiO$_2$ layers of different thickness (indicated; I, II – different samples). (a) Au($-$) – Au negatively biased, (b) Au($+$) – Au positively biased. The straight line is the best fit for the 30 nm specimen.

234

3.3. The Au(+) polarity

In this case the *I–V* characteristics cannot be transformed into good F–N plots. The linear part on the $\ln(J/U) \sim U^{-\frac{1}{2}}$ dependence, if any, covers only a couple of decades. The worse quality of the F–N plots for the Au(+) case can be due to great roughness of the oxide surface (Fig. 1). The emulsion-formed Ag electrode surface, being a replica of the oxide, repeats the rough surface relief. The curvature of individual Ag relief protrusion tips, determining the local *E* value, becomes randomly distributed. Due to this *E*-scatter, a distinctive linear F–N plot should become smeared. The scatter can be even enhanced by the percolative character of the conductivity via individual silver grains in the organic binder of the emulsion. This random walk is perceptibly manifested in the current fluctuations (noise), being by an order bigger at the Au(+) bias than in the Au(–) case.

4. CONCLUSIONS

Fowler–Nordheim tunnel currents were observed in TiO_2 films prepared by atomic layer deposition. Commonly it is thought that tunnelling field emission appears from sharp points and thin wires, concentrating the field intensity. Our results show, in accordance with [15–18], that there exist favourable conditions for the tunnelling process to appear also from virtually flat metal surfaces into a semiconductor layer.

ACKNOWLEDGEMENTS

REFERENCES

1. Khazin, L. G. *Titanium Dioxide*. 2nd ed., Leningrad, 1970 (in Russian).
2. Sheng, J., Yoshida, N., Karasawa, J. and Fukami, T. Platinum doped titania film oxygen sensor integrated with temperature compensating thermistor. *Sens. Actuators B*, 1997, **41**, 131–136.
3. Kadoshima, M., Hiratani, M., Shimamoto, Y., Torii, K., Miki, H., Kimura, S. and Nabatame, T. Rutile-type TiO_2 thin film for high-*k* gate insulator. *Thin Solid Films*, 2003, **424**, 224–228.
4. McFarland, E. W. and Jing Tang. A photovoltaic device structure based on internal electron emission. *Nature*, 2003, **421**, 616–618.
5. Repän, V., Laan, M., Paris, P., Aarik, J. and Sammelselg, V. Negative coronas: low current mode – pulse mode transition. *Czech. J. Phys.*, 1999, **49**, 217–224.

6. Vu Thien Binh and Adessi, Ch. New mechanism for electron emission from planar cold cathodes: the solid-state field-controlled electron emitter. *Phys. Rev. Lett.*, 2000, **85**, 864–867.

7. Vu Thien Binh, Dupin, J. P., Thévenard, P., Guillot, D. and Plenet, J. C. Solid-state field-controlled electron emission: an alternative to thermionic and field emission. *Mat. Res. Soc. Symp. Proc.*, 2000, **621**, R4.3.1–R4.3.6.

8. Vu Thien Binh, Semet, V. and Dupin, J. P. Novel electron sources. *Electrochem. Soc. Proc.*, 2001, **2000**, 157–166.

9. Aarik, J., Aidla, A., Mändar, H., Uustare, T. and Sammelselg, V. Anomalous effect of temperature on atomic layer deposition of titanium dioxide *J. Crystal Growth*, 2000, **220**, 531–537.

10. Aarik, J., Karlis, J., Mändar, H., Uustare, T. and Sammelselg, V. Influence of structure development on atomic layer deposition of TiO₂ thin films. *Appl. Surf. Sci.*, 2001, **181**, 339–348.

11. Ritala, M. and Leskelä, M. Zirconium dioxide thin films deposited by ALE using zirconium tetrachloride as precursor. *Appl. Surf. Sci.*, 1994, **75**, 333–340.

12. Ritala, M., Leskelä, M., Niinistö, L., Prohaska, T., Friedbacher, G. and Grasserbauck, H. Development of crystallinity and morphology in hafnium dioxide thin films grown by atomic layer epitaxy. *Thin Solid Films*, 1994, **250**, 72–80.

13. Simmons, J. G. Conduction in thin dielectric films. *J. Phys. D: Appl. Phys.*, 1971, **4**, 613–657.

14. Forbes, R. G. Refining the application of Fowler–Nordheim theory. *Ultramicroscopy*, 1999, **79**, 11–23.

15. Snow, E. H. Fowler–Nordheim tunneling in SiO₂ films. *Solid State Comm.*, 1967, **5**, 813–815.

16. Lenzlinger, M. and Snow, E. H. Fowler–Nordheim tunneling into thermally grown SiO₂. *J. Appl. Phys.*, 1969, **40**, 278–283.

17. Lewicki, G. and Mead, C. A. Currents through thin films of aluminium nitride. *J. Chem. Phys. Solids*, 1968, **29**, 1255–1267.

18. Zhirnov, V. V., Wojak, G. J., Choi, W. B., Cuomo, J. J. and Hren, J. J. Wide band gap materials for field emission devices. *J. Vac. Sci. Technol. A*, 1997, **15**, 1733–1738.

19. Fridrikhov, S. A. and Movnin, S. M. *Physical Foundations of Electronics*. Vyshaya Shkola, Moscow, 1982 (in Russian).

20. Xu, N. S., Jun Chen and Deng, S. Z. Physical origin of nonlinearity in the Fowler–Nordheim plot of field-induced emission from amorphous diamond films: thermionic emission to field emission. *Appl. Phys. Lett.*, 2000, **76**, 2463–2465.

21. Murphy, E. L. and Good, R. H., Jr. Thermionic emission, field emission, and the transition region. *Phys. Rev.*, 1956, **102**, 1464–1473.

Fowleri–Nordheimi tunneleerumine kullakihile aatomkihtsadestatud TiO₂-kiledes

Indrek Jõgi, Jaan Aarik, Viktor Bitševin, Henn Käämbre, Matti Laan ja Väino Sammelselg

Leiti, et kihtsüsteemis Au–TiO₂–Ag kuldelektroodi negatiivsel pingestamisel titaandioksiidi kilesid läbivaid voole kirjeldab hästi Fowleri–Nordheimi valem (1), mis on tuletatud metallteravikest ning juustraatidest vaakumisse kiirguva väljaemissiooni jaoks, kuid kehtib ka uuritud kihistikus. Valemi (1) kehtivus näitab, et tegemist on tunnelvooludega, mida põhjustab tõenäoselt tunnelefekt läbi Au ja TiO₂ vahelisel lahutuspinnal tekkiva Schottky barjääri (vt joonis 4). Tulemus on heas kooskõlas varasemates töödes [15–18] tehtud mõõtmistega, milles leiti seost (1) järgivad tunnelvoolud SiO₂- ja AlN-kiledes, ning äsjaste tulemustega magnetronpihustatud TiO₂-kiledes [3] .

236